





Subsurface Metallic Object Detection Using GPR Data and YOLOv8 Based Image Segmentation

Duarte Branco^{1,2}^a, Rui Coutinho^{1,2}^b, Armando Sousa^{1,2}^c, and Filipe dos Santos²^d

¹Faculty of Engineering (FEUP), University of Porto, Rua Dr. Roberto Frias, Porto, Portugal

²INESC Technology and Science (INESC TEC), Rua Dr. Roberto Frias, Porto, Portugal

fi

Keywords: Ground Penetrating Radar, GPR, Object Detection, Subsurface Characterization, YOLO, Hyperbola Model.

Abstract: Ground Penetrating Radar (GPR) is a geophysical imaging technique used for the characterization of a subsurface's electromagnetic properties, allowing for the detection of buried objects. The characterization of an object's parameters, such as position, depth and radius, is possible by identifying the distinct hyperbolic signature of objects in GPR B-scans. This paper proposes an automated system to detect and characterize the presence of buried objects through the analysis of GPR data, using GPR and computer vision data processing techniques and YOLO segmentation models. A multi-channel encoding strategy was explored when training the models. This consisted of training the models with images where complementing data processing techniques were stored in each image RGB channel, with the aim of maximizing the information. The hyperbola segmentation masks predicted by the trained neural network were related to the mathematical model of the GPR hyperbola, using constrained least squares. The results show that YOLO models trained with multi-channel encoding provide more accurate models. Parameter estimation proved accurate for the object's position and depth, however, radius estimation proved inaccurate for objects with relatively small radii.

1 INTRODUCTION

The characterization of a subsurface is an intrinsic problem in many fields of science and engineering, essentially everywhere there is a need to determine what is beneath a visually opaque surface. Naturally, non-destructive and non-intrusive techniques to solve this problem are of great importance, where there is a need to preserve the probing environment.


In this context, Ground Penetrating Radar (GPR) has emerged as one of the most useful subsurface probing methods. In essence, GPR is able to characterize the electromagnetic response of a subsurface, allowing for the detection of buried objects. Object detection and characterization are possible by identifying and analysing the distinct hyperbolic signature of an object in GPR data ((Persico, 2014; Utsi, 2017; Jol, 2009; Daniels, 2004)).


Traditionally, this process requires human interpretation of the GPR data. However, analysing GPR


data is a difficult operation that requires relevant knowledge of the operating principles of GPR, the propagation of electromagnetic waves, and their interactions with the subsurface and buried objects ((Persico, 2014; Utsi, 2017; Jol, 2009; Daniels, 2004)). For this reason, research has focused on systems to model and analyze GPR data.


In general, these systems include a data processing step followed by a hyperbola detection step and parameter estimation considering the model of a GPR hyperbola ((Zhou et al., 2018)).

The data processing step has the goal of mitigating the effect of noise, cluttering signals and attenuation, such that the hyperbola signature is easier to identify. Traditional GPR data processing techniques include dewow, timezero correction, frequency filtering, deconvolution, background removal and gain ((Persico, 2014; Utsi, 2017; Jol, 2009; Daniels, 2004)). Recently, other approaches based on subspace methods and deep-learning have been proposed. Subspace-based methods include singular value decomposition, principal component analysis and independent component analysis (Chen et al., 2019). In essence, these aim to project the original B-scan data onto clutter and target subspace. Deep learning methods con-

^a <https://orcid.org/0009-0006-2039-8492>

^b <https://orcid.org/0000-0001-8821-2224>

^c <https://orcid.org/0000-0002-0317-4714>

^d <https://orcid.org/0000-0002-8486-6113>

sist in training neural networks, namely autoencoders ((Bestagini et al., 2020)) or Generative Adversarial Nets (GANs) ((Ni et al., 2022)), to predict a noise-free image.

Computer vision techniques have been used to filter noise and detect the hyperbola, using noise filtering, thresholding, morphological operations and edge detection based approaches ((Zhou et al., 2018)).

Several different types of machine learning algorithms and neural networks have been used for the task of hyperbola detection, including support vector machines, classification models, different architectures of convolutional neural networks and adversarial neural networks ((Bai et al., 2023)). The You Only Look Once (YOLO) family of networks is one of the more advanced one-stage detection models ((Zheng et al., 2023)), making it a compelling tool for hyperbola detection.

The goal of this paper is to implement a system to detect and characterize objects in GPR data with an approach based on exploring the training of YOLO models by exploring a multi-channel encoding strategy. Multi-channel encoding consists in storing different information in each of the three image RGB colour channels. Thus, it's possible to take full advantage of the YOLO networks, which support inputs with three channels, by providing it with multiple B-scans images, where different processing techniques were applied, and combined in an RGB image.

The article starts by introducing background concepts related to GPR operation and data analysis. Next, the developed system is described in depth and its results are exposed. Finally, the results are discussed and the performance of the system is evaluated.

2 BACKGROUND

The working principles of GPR operation are similar to those of conventional radar but applied to a different probing medium, the subsurface ((Persico, 2014; Utsi, 2017; Jol, 2009; Daniels, 2004)). The most common configuration of GPR systems consists of a transmitter and receiver antenna in a fixed geometry, which is moved over the surface in order to probe it. Essentially, GPR works by transmitting electromagnetic waves into the subsurface, which are then scattered and/or reflected by changes in the medium's electromagnetic properties which are caused by dielectric discontinuities. The reflected waves are picked up by the receiver antenna, allowing for the characterization of the medium and the buried objects' depth and geometry. Depth is determined

by the time interval between the transmission and reception of the electromagnetic (EM) waves and their propagation velocity, which depends on the medium's EM properties. This is expressed by equation 1.

$$d = v \frac{t}{2} \quad (1)$$

In simple terms, since reflection depends on the object's electrical and magnetic properties, this means that GPR can detect any material provided these properties are sufficiently different from its surrounding materials.

GPR data can be represented in different ways. An A-scan is the representation of a single reflected EM wave on a time-amplitude graph, plotted along an axis which represents the wave's travel time, which is proportional to depth. The aggregation of consecutive A-scans measured along a fixed direction, in this case, the x-axis, results in a B-scan. The resulting B-scan can be interpreted as a two-dimensional (2D) image where the EM waves' amplitude is represented using brightness or colour modulation.

The signals transmitted by GPR antennas propagate as ellipses with increasing areas as they propagate deeper, resulting in a beam with an elliptical cone shape. This phenomenon is described by equation 2, where $E/2$ represents the energy radius, H the propagation distance, ϵ_r the relative permittivity and λ the signal's wavelength ((Chang et al., 2009)). This in turn will result in the reflection, and subsequent recording, of EM waves before and after the GPR is directly above the object of interest.

$$\frac{E}{2} = \frac{\lambda}{4} + \frac{H}{\sqrt{\epsilon_r + 1}} \quad (2)$$

When the GPR is directly above the object the EM waves will be reflected along the direct path, corresponding to the object's depth. Before and after this, the object will be detected via a longer path, resulting in a longer time interval between the transmission and recording of the EM wave. If the object is cylindrical and perpendicular to the scan's direction, when plotted in a B-scan, this behaviour will result in a hyperbolic shape. The hyperbole's apex indicates the object's depth, since it's created by the EM wave reflected when GPR is directly above the object.

In essence, the GPR hyperbola can be modelled mathematically by the geometrical parameters of the scan and the time an EM wave takes to be reflected. This model assumes some simplifications, namely, a null offset between the GPR antennas, null distance between the surface and the GPR, a homogeneous medium with constant EM wave propagation velocity and a cylindrical object buried perpendicular to the scan's direction ((Chen and Cohn, 2010)).

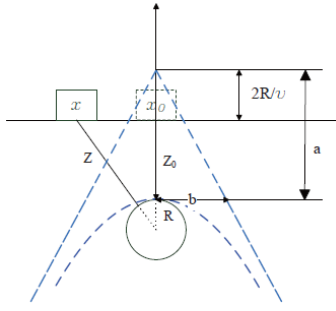


Figure 1: GPR hyperbola model of a cylindrical object, considering zero antenna offset, and the relationship with the scan's geometrical parameters (Chen and Cohn, 2010).

Considering figure 1, where Z and Z_0 represent the distance travelled by the EM wave to an object of radius R , and equation 1:

$$(x - x_0)^2 + (Z_0 + R)^2 = (Z + R)^2 \quad (3)$$

$$(x - x_0)^2 + \left(\frac{vt_0}{2} + R\right)^2 = \left(\frac{vt}{2} + R\right)^2$$

By re-writing the previous expression, the GPR hyperbola model can be represented by the general hyperbola equation, given by equation 4. Thus, equation 3 is re-written as equation 5.

$$\frac{(y - y_0)^2}{a^2} - \frac{(x - x_0)^2}{b^2} = 1 \quad (4)$$

$$\frac{(t + 2R/v)^2}{(t_0 + 2R/v)^2} - \frac{(x - x_0)^2}{(vt_0/2 + R)^2} = 1 \quad (5)$$

$$a = t_0 + \frac{2R}{v} \Leftrightarrow t_0 = a - \frac{2R}{v} \quad (6)$$

$$b = v \frac{t_0}{2} + R \quad (7)$$

$$y_0 = \frac{2R}{v} \quad (8)$$

Following these equations, an object's position corresponds to the horizontal position of the hyperbola apex, x_0 , and the depth is from the reflection time, t_0 , and equation 1. The remaining parameters, namely, the object's radius and EM wave velocity are related to the hyperbola parameters, by the following equations:

$$v = \frac{2b}{a} \quad (9)$$

$$R = \frac{v(a - t_0)}{2} \Leftrightarrow R = \frac{b(-y_0)}{a} \quad (10)$$

Consequently, by fitting the parameters of the mathematical hyperbola model it's possible, namely a , b , x_0 and y_0 , it's possible to determine the object's

parameters and wave velocity. Fitting has been defined following a constrained least-squares minimization problem ((Zhou et al., 2018)).

While the hyperbola fitting process works well for well-shaped hyperbolas ((Mertens et al., 2015; Giannakis et al., 2022)), in real GPR data hyperbolas are often miss-shaped. In these conditions, the parameters estimated will be affected by an error, since they will be estimated by noisy points. In particular, the effect of noise is heavily detrimental to an accurate radius estimation. The remaining parameters, namely, EM wave velocity and object depth and position can be sufficiently estimated even considering noise.

Considering this, the radius can be estimated through an alternative method, proposed in (Chang et al., 2009). This method relates the number of A-scans where a reflection is detected, given by the hyperbola width, L , and the energy radius, expressed in equation 2. Thus, the radius is given by:

$$S = L - E \quad (11)$$

$$R = \frac{S}{2\pi} \quad (12)$$

3 METHODOLOGY

The system's architecture is characterized by three main components: Image processing, Hyperbola detection and Hyperbola fitting. Image processing was done using both GPR and computer vision processing techniques, with the goal of making it easier to identify hyperbolic patterns. Hyperbola detection is achieved using a YOLOv8 segmentation neural network, trained with images with different processing techniques in each image colour channel. Hyperbola fitting was done using the segmentation masks provided by the network, with the goal of estimating the object's parameters using the GPR hyperbola model. This step also includes a hyperbola mask processing component, used to determine the hyperbola fitting points. The high-level architecture of the system is illustrated in figure 2.

3.1 Dataset Creation

A dataset comprising 294 GPR B-scans was collected and annotated, which was further augmented using image augmentation techniques, in order to train the neural networks. The original scans were split into training, testing and validation subsets, following an 80%, 10%, and 10% splits, respectively. The augmentation techniques in CLAHE, flipping, resizing and

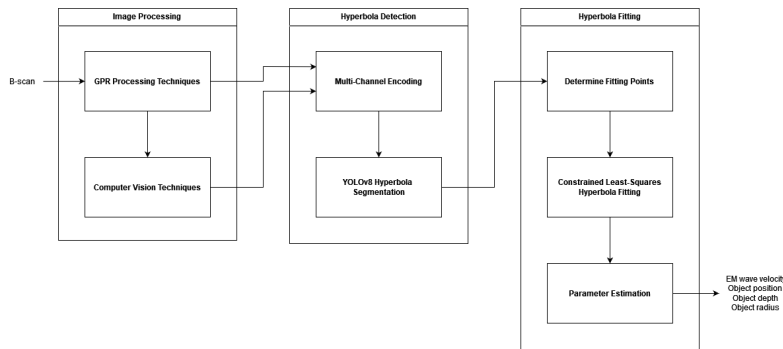


Figure 2: System architecture.

rotation ((Shorten and Khoshgoftaar, 2019)). In order to generate a greater number of images, all combinations of these techniques were applied to the original image and between the augmented images, with the exception of resize and rotation. These were only applied to images with at least one other technique. After applying these transformations 8 images were generated from an original scan. Augmentation was applied to the training and validation datasets. A second smaller dataset with the object’s, composed of 30-B-scans, depth and position ground-truth was collected, in order to verify the precision of the developed system. For both datasets, objects consisted of solid metallic cylinders with radii of 0.5, 1.4 and 1.5 cm. Scans were taken following straight lines where objects were buried in soil perpendicular to the direction of the scan. The GPR equipment used was OERAD’s Concretto GPR system.

Data will be made available upon the acceptance of the paper.

3.2 Data Processing and YOLOv8 Training

A sequential pipeline composed of the following GPR processing techniques was applied to every scan: dewow, mean background removal and band-pass filter. The dewow window was set correspond to the GPR pulse length and the cutoff frequencies of the band-pass filter to correspond to the spectrum of the GPR system. After this, the following processing techniques were applied. Automatic gain control (AGC), with a window set to correspond to the pulse length, was implemented to mitigate the attenuation effect. Computer vision techniques included template matching, implemented through the normalized cross-correlation (NCC) of A-scans with a pulse reference signal, and a Sobel edge detection filter. These processes are illustrated in figure 3.

Different processing techniques were stored in

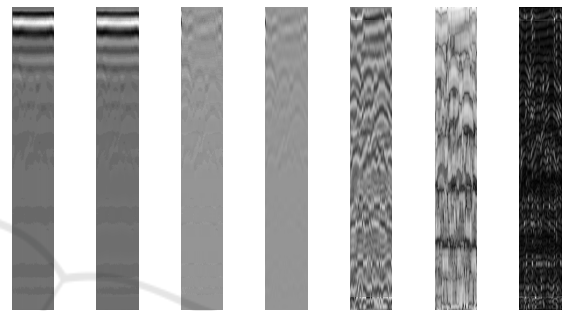


Figure 3: GPR processing applied to a B-scan (Left to right): Original, Dewow, Background removal, Bandpass filter, AGC, NCC, Sobel.

each RGB image channel, chosen with the goal of providing complementary information to the neural network. These multi-channel encoding configurations are listed in table 1.

Table 1: Multi-channel encoding configurations (MCEC) of different B-scan processing techniques, stored in the image’s BGR channels.

MCEC	B	G	R
1	GPR Processing	GPR Processing	GPR Processing
2	GPR Processing	AGC	-
3	GPR Processing	NCC	-
4	GPR Processing	Sobel	-
5	GPR Processing	AGC	NCC
6	GPR Processing	AGC	Sobel
7	AGC	AGC	AGC
8	AGC	NCC	-
9	AGC	Sobel	-
10	AGC	NCC	Sobel
11	NCC	NCC	NCC
12	Sobel	Sobel	Sobel

YOLOv8 nano models were trained for each configuration, in order to determine which provided the best results. Then a YOLOv8 medium model was trained in order to determine if better results could be obtained with a more complex model. These models were trained for 40 and 20 epochs, respectively, using the default training hyperparameters, with the exception of the learning rate, 0.0001, batch-size, 24,

dropout, 0.2, optimizer, *SGD* and early stopping disabled. After training, the best model was implemented in the complete system to determine the hyperbola segmentation masks. The YOLO predictions are illustrated in figure 4.

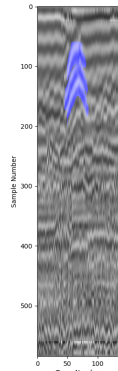


Figure 4: YOLO hyperbola mask predictions from the trained YOLO model implemented in the system.

3.3 Model Fitting

The segmentation masks obtained from the YOLO model were processed by an algorithm, in order to obtain the points used in the fitting procedure. Since YOLO predictions could be ill-shaped hyperbola masks, the algorithm was used to determine the correct hyperbola branches by considering the skeletonized mask. The algorithm worked by determining the intersection points where multiple skeleton branches connected, and then determining the biggest continuously connected branches, which would match the actual hyperbola branches. Taking into account the hyperbola's shape, branches which would have a horizontal overlap weren't considered when verifying branch connections. After determining the skeleton which effectively describes the hyperbola, the fitting points are obtained by considering the mean point in each branch.

The fitting problem was defined as a constrained least-squares problem, based on what's described in (Zhou et al., 2018). The general hyperbola equation can be re-written as:

$$\begin{cases} \frac{(y-y_0)^2}{a^2} - \frac{(x-x_0)^2}{b^2} = 1 \\ -\frac{a^2}{b^2}x^2 + y^2 + 2\frac{a^2}{b^2}x_0x - 2y_0y + y_0^2 - a^2 - \frac{a^2}{b^2}x_0^2 = 0 \end{cases} \quad (13)$$

Thus, the problem function can be represented by the following equations, which relate the fitting coefficients with the hyperbola parameters:

$$F(i) = a_c x^2 + b_c xy + c_c y^2 + d_c x + e_c y + f_c = 0 \quad (14)$$

$$\begin{cases} a^2 = \left(\frac{e_c}{2}\right)^2 - f_c + \frac{d_c^2}{4a_c} \\ b^2 = \frac{(-e_c/2)^2 - f_c - d_c}{a_c} \\ x_0 = \frac{d_c}{-2a_c} \\ y_0 = \frac{-e_c}{2} \end{cases} \quad (15)$$

Given the physical restrictions on the parameters associated with the scan, it's necessary to constrain the minimization problem. Consecutively, bearing in mind equations 9 and 10 and the system of equations 15, the coefficients are constrained such that the minimum radius was half of our GPR's horizontal resolution, 0.5mm, and velocity had a positive value smaller than the speed of light in vacuum. The fitting process was implemented using the Pyomo software package ((Hart et al., 2011)) and the IPOPT solver ((Wächter and Biegler, 2006)).

Finally, the scan's parameters were determined. Due to the fact that the radius determined from hyperbola fitting is heavily affected by miss-shaped hyperbolas, the radius was calculated using the energy radius method. The hyperbola width was obtained from the width of the segmentation mask or from double the distance from the x position of the determined apex to the furthest x coordinate of a point belonging to the fitted points. The biggest of these distances would be considered the hyperbola's width. This was done with the goal of mitigating the effect of asymmetric segmentation masks, where the full length of both of the hyperbola branches wouldn't be detected, such that the mask's width wouldn't effectively correspond to the actual width of the hyperbola. Additionally, it was observed that multiple hyperbolic reflections were created by an object. This is due to the ringing effect, caused due to signals repeatedly bouncing within an object, which usually occurs in metallic objects ((Persico, 2014; Utsi, 2017; Jol, 2009; Daniels, 2004)). Consequently, all of the hyperbolas from an object were grouped given their apexes similar x position. The first-hyperbola, that is, the one with smaller depth, correctly indicated the objects depth, while the repetitions echos, gave an exaggerated depth. All of the parameters were calculated from the first hyperbolic reflection and also from a mean of the parameters considering the first hyperbola and its echos, and the results were compared. This was done with the goal of trying to take advantage of the multiple hyperbola reflections and obtaining a more accurate result, by mitigating the effect of a miss-shaped hyperbola in the fitting process.

The fitting results are illustrated in figure 5.

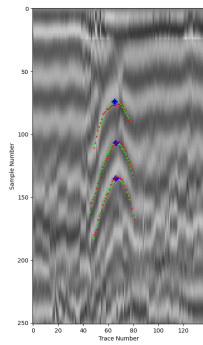


Figure 5: Constrained least-squares fitting of GPR hyperbola model of a B-scan. Fitting points are shown in red, fitting results are shown in green and the hyperbola apex is shown in blue. Due to the ringing effect multiple hyperbolas are observed.

4 RESULTS

A concise summary of the YOLO model evaluation metrics for the testing dataset is shown in table 2. By analysing the evaluation metrics of the segmentation masks, in particular the precision, recall, mAP50 and mAP50-95, it's possible to compare the different models. For the sake of conciseness, each multi-channel encoding strategy is referred to by its configuration, as listed in table 1.

Multi-channel configuration 6 stands out due to its good performance both in the validation and testing data. This configuration achieves the highest results in many of the metrics and closely matches other configurations when it's not the best. Notably, its robustness to false positives, given by the recall, stands out in the testing dataset. The precision value, mAP50 and mAP50-95 are also some of the highest. For these reasons, multi-channel encoding configuration 6 was considered the best.

Next, a YOLOv8 medium model was trained with this configuration. The metrics from training and validation per epoch are illustrated in figure 7. The results after training was concluded are shown in table 3. Considering the improved results in the recall, mAP50, mAP50-95 and fitness for the testing dataset, when compared to the YOLOv8 nano segmentation model trained with the same multi-channel encoding configuration, this model was used in the final system. Considering the F1-score-confidence curve, a confidence threshold of 0.15, was used to accept a prediction. This rather low value was chosen since it was considered more detrimental to have missed detections rather than false positives.

In order to evaluate the success of the whole system in estimating the scan's parameters, the sys-

tem verification dataset was used. As previously mentioned, the parameters were obtained considering only the first hyperbola, and the first hyperbola and all its repetitions.

The absolute error for the estimated parameters is shown next. In order to better represent the estimation error, some considerations were taken, such that the estimated parameters are valid and the error properly indicated the accuracy of estimation. For the position error, all of the scans were considered when calculating, since at least one true-positive hyperbola was detected in all scans. For the depth error, only scans where the first-hyperbola was correctly labelled were considered. For the radius error, the previous consideration was also used as well as the radius being greater than zero, since otherwise it would indicate that the hyperbola's width wasn't properly determined.

5 CONCLUSION

In this paper, a system for object detection and characterization in GPR data was implemented, which used YOLOv8 segmentation model for hyperbola detection and constrained least-squares fitting considering the GPR hyperbola model. The approach explored the combination of different data processing techniques via a multi-channel encoding strategy that had the goal of providing the model with a B-scan image where complementing processing techniques were applied. These techniques consisted of both traditional GPR processing and also computer vision methods.

In order to determine which multi-channel configuration produced the best detection results, multiple YOLOv8 segmentation nano models were trained and their metrics were compared. This analysis concluded that the best multi-channel encoding configuration consisted of the GPR processing steps, AGC and Sobel filter. Next, a YOLOv8 segmentation medium model was trained with this configuration achieving improved results, thus being implemented in the final system.

The segmentation masks provided by the trained model were processed, to obtain the correct hyperbola branches from masks with potentially ill-shaped masks. Next, constrained least squares was used to obtain the hyperbola's parameters considering the hyperbola model. The scan's parameters, namely, the object's position, depth and radius, and the medium's EM wave propagation velocity were then estimated, considering only the first-hyperbola, and the first-hyperbola and its repetitions.

Table 2: Testing metrics of YOLOv8 segmentation nano models on multi-channel encoding configurations (MCEC).

MCEC	Precision	Recall	mAP50	mAP50-95	Fitness
1	0.8940	0.7063	0.8100	0.3140	0.8730
2	0.9219	0.6650	0.8135	0.3022	0.8722
3	0.7726	0.5714	0.6715	0.2236	0.6664
4	0.8172	0.6798	0.7828	0.2854	0.8226
5	0.8369	0.6650	0.7856	0.2863	0.8143
6	0.9136	0.7340	0.8382	0.3080	0.8776
7	0.9219	0.6650	0.8135	0.3022	0.8722
8	0.7757	0.6643	0.7561	0.2744	0.7798
9	0.8546	0.6897	0.8214	0.3088	0.8640
10	0.8283	0.6700	0.7623	0.2814	0.8043
11	0.7806	0.5783	0.6721	0.2006	0.6401
12	0.5793	0.5468	0.5296	0.1491	0.5416

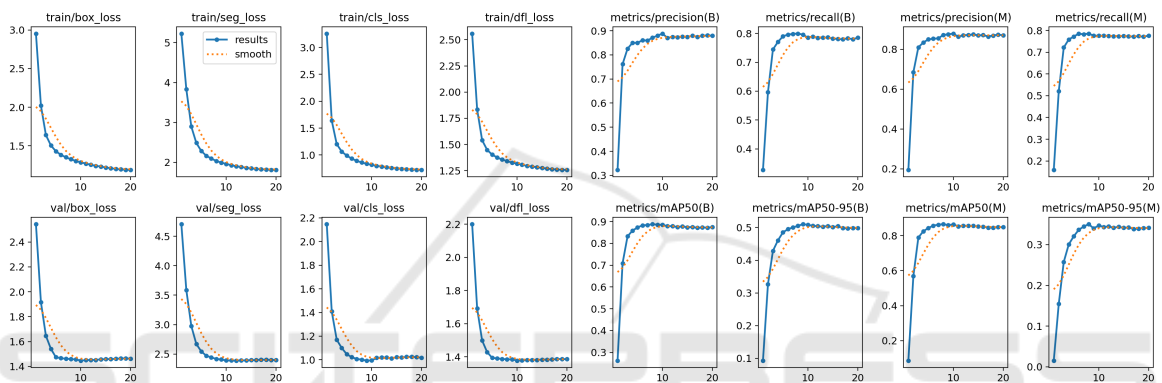


Figure 6: Training and validation results of YOLOv8 segmentation medium model on multi-channel encoding configuration 6.

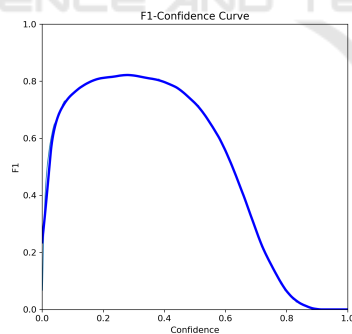


Figure 7: F1-score confidence curve considering validation dataset on YOLOv8 segmentation medium model on multi-channel encoding configuration 6.

Table 3: Validation and testing metrics of YOLOv8 segmentation medium model on multi-channel encoding configuration 6.

Metric	Validation Dataset	Testing Dataset
Precision	0.8801	0.8624
Recall	0.7733	0.7931
mAP50	0.8617	0.8770
mAP50-95	0.3461	0.3339
Fitness	0.9372	0.9394

The error values of the estimated parameters show that an accurate result can be obtained for the position and depth estimates. The results obtained considering the hyperbola repetitions indicate that this method can obtain a more accurate depth estimate. This is essentially due to a better velocity estimate when considering the mean of multiple estimates of repeated hyperbolas. Similar error values occur for the position estimate, considering both methods, which indicate that the position when estimated from the average of multiple hyperbola repetitions is also valid. However, rather high results for radius are present, noting that the objects used had radii of 0.5, 1.4 and 1.5 cm. Error in estimation velocity or hyperbola apex position will affect the calculation of the energy radius, due to the effect on estimated depth. Additionally, an error in the value of the hyperbola’s width will also affect the radius calculation.

The success of the entire system essentially depends on the good performance of the YOLO model. If the mask predictions don’t effectively match the hyperbola’s shape the estimation of all of the parameters will be affected. Additionally, the system is also affected by false positive and false negative detections.

Table 4: Average absolute error, Δ , of valid estimated parameters. Medium's EM wave propagation velocity, v , and object's position, x , depth, y , and radius, r . Calculated considering only first-hyperbola, $1st$, and all hyperbolas from an object, $group$.

Δx_{1st} (cm)	Δx_{group} (cm)	Δy_{1st} (cm)	Δy_{group} (cm)	Δr_{1st} (cm)	Δr_{group} (cm)
2.7	2.9	2.3	1.4	0.4	0.6

The developed system works as expected when hyperbola segmentation provided well-fitting masks, such that the parameters were estimated from fitting points which correctly described the hyperbola.

ACKNOWLEDGEMENTS

This work is co-financed by Component 5 - Capitalization and Business Innovation, integrated in the Resilience Dimension of the Recovery and Resilience Plan within the scope of the Recovery and Resilience Mechanism (MRR) of the European Union (EU), framed in the Next Generation EU, for the period 2021 - 2026, within project AgendaTransform, with reference 34.

REFERENCES

- Bai, X., Yang, Y., Wei, S., Chen, G., Li, H., Li, Y., Tian, H., Zhang, T., and Cui, H. (2023). A comprehensive review of conventional and deep learning approaches for ground-penetrating radar detection of raw data. *Applied Sciences*, 13(13):7992.
- Bestagini, P., Lombardi, F., Lualdi, M., Picetti, F., and Tubaro, S. (2020). Landmine detection using autoencoders on multipolarization GPR volumetric data. *IEEE Transactions on Geoscience and Remote Sensing*, 59(1):182–195.
- Chang, C. W., Lin, C. H., and Lien, H. S. (2009). Measurement radius of reinforcing steel bar in concrete using digital image gpr. *Construction and Building Materials*, 23(2):1057–1063.
- Chen, G., Fu, L., Chen, K., Boateng, C. D., and Ge, S. (2019). Adaptive ground clutter reduction in ground-penetrating radar data based on principal component analysis. *IEEE Transactions on Geoscience and Remote Sensing*, 57(6):3271–3282.
- Chen, H. and Cohn, A. (2010). Probabilistic robust hyperbola mixture model for interpreting ground penetrating radar data. *Proceedings of the International Joint Conference on Neural Networks*, pages 1–8.
- Daniels, D. J. (2004). *Ground Penetrating Radar, 2nd Edition*. Institution of Electrical Engineers, London, United Kingdom.
- Giannakis, I., Zhou, F., Warren, C., and Giannopoulos, A. (2022). On the limitations of hyperbola fitting for estimating the radius of cylindrical targets in nondestructive testing and utility detection. *IEEE Geoscience and Remote Sensing Letters*, 19:1–5.
- Hart, W. E., Watson, J.-P., and Woodruff, D. L. (2011). Pyomo: modeling and solving mathematical programs in python. *Mathematical Programming Computation*, 3(3):219–260.
- Jol, H. M. (2009). *Ground Penetrating Radar Theory and Applications*. Elsevier Science, Amsterdam, Netherlands.
- Mertens, L., Persico, R., Matera, L., and Lambot, S. (2015). Automated detection of reflection hyperbolas in complex gpr images with no a priori knowledge on the medium. *IEEE Transactions on Geoscience and Remote Sensing*, 54(1):580–596.
- Ni, Z.-K., Shi, C., Pan, J., Zheng, Z., Ye, S., and Fang, G. (2022). Declutter-gan: Gpr b-scan data clutter removal using conditional generative adversarial nets. *IEEE Geoscience and Remote Sensing Letters*, 19:1–5.
- Persico, R. (2014). *Introduction to Ground Penetrating Radar: Inverse Scattering and Data Processing*. John Wiley and Sons, Inc., Hoboken, New Jersey.
- Shorten, C. and Khoshgoftaar, T. M. (2019). A survey on image data augmentation for deep learning. *Journal of Big Data*, 6:1–48.
- Utsi, E. C. (2017). *Ground Penetrating Radar: Theory and Practice*. Butterworth-Heinemann, Oxford, United Kingdom.
- Wächter, A. and Biegler, L. T. (2006). On the implementation of a primal-dual interior point filter line search algorithm for large-scale nonlinear programming. *Mathematical Programming*, 106(1):25–57.
- Zheng, X., Fang, S., Chen, H., Peng, L., and Ye, Z. (2023). Internal detection of ground-penetrating radar images using yolox-s with modified backbone. *Electronics*, 12(16):3520.
- Zhou, X., Chen, H., and Li, J. (2018). An automatic gpr b-scan image interpreting model. *IEEE Transactions on Geoscience and Remote Sensing*, 56(6):3398–3412.